Impacts of hydrodynamic conditions and surface roughness on the critical condition to develop and thickness of *Pseudomonas putida* biofilms

Guanju Wei [1, 2], *Judy Q. Yang* [1, 2*]

[1]Saint Anthony Falls Laboratory, University of Minnesota, Minneapolis MN, USA; [2]Department of Civil, Environmental, and Geo-Engineering

KEYWORDS: biofilm, hydrodynamic conditions, surface roughness, critical conditions, thickness, microfluidics

ABSTRACT: The formation of biofilms can increase pathogenic contamination of drinking water, cause biofilm-related diseases, and alter the rate of sediment erosion in rivers and coasts. Meanwhile, some biofilms have been used in moving-bed biofilm reactors (MBBRs) to degrade contaminants in wastewater. Mechanistic understanding of biofilm formation is critical to predict and control biofilm development, yet such understanding is currently incomplete. Here, we reveal the impacts of hydrodynamic conditions and surface roughness on the formation of *Pseudomonas putida* biofilms through a combination of microfluidic experiments, numerical simulations, and fluid mechanics theories. We demonstrate that biofilm growth is suppressed under high flow conditions and characterize the local critical velocity for *P. putida* biofilms to develop, which is about 50 μm/s. We further demonstrate that micron-scale surface roughness promotes biofilm formation by increasing the area of low-velocity region. Furthermore, we show that the critical shear stress, above which biofilms cease to form, for biofilms to develop on rough surfaces is 0.9 Pa, over 3 times higher than that for flat surfaces, 0.3 Pa. The results of this study will facilitate future predictions and control of biofilm development on surfaces of drinking water pipelines, blood vessels, sediments, and MBBRs.

INTRODUCTION

Biofilms, consortiums of bacterial cells and extracellular polymeric substances (EPS) attached to surfaces[1], are ubiquitous in rivers[2-4], coastal areas[5], human organs[6], and drinking water distribution systems (DWDS)[7, 8]. Many biofilms are harmful because they increase the presence of pathogenic bacteria in DWDS[9], clog medical devices[10-12], and increase bacterial resistance to bactericides[13]. Many other biofilms, such as those used in moving-bed biofilm reactors (MBBRs)[14], are beneficial as they remove harmful organic compounds and nutrients from waste-water[15]. Biofilm thickness is a key parameter to characterize biofilms because it determines when clogging occurs and the efficiency of biofilm-based wastewater treatment plans[16, 17]. The critical condition, above which biofilm thickness becomes zero, is another key parameter because it informs strategies to prevent or control biofilm development. Systematic studies about factors that control biofilm thickness and the critical conditions for biofilm to develop are needed yet currently lacking.

Hydrodynamic conditions and surface roughness are two important factors that control biofilm growth[18-20], yet their impacts remain controversial. First, some studies show that high flow velocity or shear favors biofilm growth, increases biofilm thickness, and gives rise to a more elastic and resistant biofilm[21, 22]. In contrast, some other studies show that high flow conditions reduce the thickness of biofilms in bioreactors[23]. Systematic investigation is needed to reveal the impacts of flow on biofilm development. Second, many studies show that surface roughness increases bacterial adhesion and facilitates biofilm formation[24-26]. In contrast, some other studies show that higher surface roughness reduces bacterial adhesion and biofilm density[27, 28]. Systematic investigation of biofilm development on rough surfaces with different roughness heights and shapes is also important, because rough surfaces are ubiquitous in natural and

artificial environments, e.g., the surfaces of river sediment bed[29, 30], drinking water pipelines[31], and MBBRs[32, 33]. Therefore, to prevent harmful biofilms and make use of beneficial biofilms, mechanistic understanding of the combined effects of hydrodynamic conditions and surface roughness on biofilm formation, especially biofilm thickness and the critical conditions to develop biofilms, is needed yet currently remains incomplete.

Here we investigate the impacts of hydrodynamic conditions and surface roughness on the formation of *Pseudomonas putida* biofilms. *P. putida* is a bacterium commonly found on the surfaces of aquatic sediment[34], terrestrial soils[35], and drinking water systems[36]. In addition, *P. putida* has been widely used in bioremediation[37] due to its capability to degrade a wide variety of contaminants including lignin[38, 39], heavy metals[40, 41] and phenols[42]. Fundamental understanding of the factors that control the formation of *P. putida* biofilms is critical for reducing biofilm contamination of our aquatic and terrestrial environments as well as improving the efficiency of biofilm-based bioremediation projects. In this study, we combine biofilm development experiments in custom-designed microfluidic channels with COMSOL simulation and fluid mechanics theories to evaluate the impacts of hydrodynamic conditions and surface roughness on the critical shear stress, above which *P. putida* biofilms cease to form, and the thickness of these biofilms. First, we quantify the impact of flow velocity on biofilm thickness. Second, we quantify the impacts of surface roughness, including its height and shape, on biofilm thickness. Third, we quantify the impacts of surface roughness on the critical shear stress above which biofilms cease to develop. Finally, we discuss the implications of our results in the prediction and control of biofilms in natural aquatic and terrestrial environments, drinking water systems, and biofilm-based reactors used in bioremediation.

MATERIALS AND METHODS

Bacterial Strains and Culture. First, we cultured *Pseudomonas putida* KT2442 (a gift from Mohamed Donia's lab, Princeton University) cells from frozen stocks in LB solution overnight (around 16 hours) in an incubator with 200 rpm shaking rate at 30 °C. Second, we transferred the cells in the growth phase to modified M9 solution which has fully characterized chemical composition. Specifically, we centrifuged the 5 mL bacterial cultures in 50 mL tubes at 4,000 rpm for 10 minutes, after which, we removed the supernatant (LB) from the tube. Then, the bacteria deposit were diluted by M9 medium solution until the OD_{600} was approximately 0.5. The M9 medium solution was supplemented with micronutrients (0.03 M $(NH_4)_6(Mo_7)_{24}$, 4 M H_3BO_3, 0.3 M $CoCl_2$, 0.1 M $CuSO_4$, 0.8 M $MnCl_2$, 0.1 M $ZnSO_4$, and 0.1 M $FeSO_4$) in this study. The carbon source we used here is D-glucose at 1 wt. % concentration.

Experimental Platform and Biofilm Development Experiment. Microfluidic experiments were conducted to characterize development of biofilms on varying surfaces at different flow rates. Schematic diagram of the microfluidic platform is shown in Figure S1. The system consists of a microfluidic chip, a confocal laser scanning microscope (Nikon C2 plus) and a syringe pump (PHD Ultra, Harvard Apparatus). Soft lithography was used to fabricate microfluidic chips. First, we created a mold for the channel on an SU-8-coated silicon wafer using LaserWriter-Heidelberg DWL-200 at the University of Minnesota Nano Center. Afterwards, we created the microfluidics by pouring polydimethylsiloxane (PDMS) with curing agent (Sylgard 184, Dow Corning) onto the molded silicon wafer. After curing the PDMS on a 100 °C hotplate for about one hour, we removed the PDMS from the silicon wafer and punched holes at the channel inlet and outlet with a 1 mm puncher (Med Blades). Then, we bonded the PDMS to a #1.5 cover glass

after treating the two bonding surfaces with Asher-Oxygen etcher. The total height of all channels used in this study is 60 μm and the width is 400 μm. The channel measures approximately 5 mm in length from inlet to outlet. During the experiment, the chips were placed on the stage top incubator (UNO-T-H, Okolab) with controlled temperature (30 °C). A syringe pump (PHD Ultra, Harvard Apparatus) is used to precisely control the injection flow rate of the glucose solution. Confocal microscopy was used to image the microfluidic channels and biofilms with 0.31 μm/pixel resolution.

Biofilm development experiments were conducted following the steps described below. First, we injected 5 ml *Pseudomonas putida* solution with $OD_{600} \approx 0.5$ (overnight cultures diluted with M9 solution) into the microfluidics manually with flow rate on the order of mL/min. Afterwards, we switched the three-way valve and injected abiotic M9 solution containing 1 wt. % glucose at different flow rates, from 1 μL/min to 125 μL/min, to the channel using 3 ml/10 ml/100 ml syringes for 24 hours. As the cells grow and develop biofilms on the side walls of the channel (see Figure S1 for details), we recorded the images of biofilms using a confocal microscope at 30-minute intervals. To demonstrate the cells release EPS to form biofilms, we stained the EPS to visualize the biofilms. See the supporting information (SI, Figure S2) for more details.

Microfluidic Channel Pattern Design. To evaluate the impacts of roughness height and geometry on biofilm development, we designed microfluidic channels with three roughness heights and two roughness geometries, round and angular, to represent typical geometries of drinking water pipelines and sediment in natural rivers[43, 44]. The roughness elements were placed at the lower boundary of our microfluidics channel (Figure S1). The upper boundary of our

microfluidics channel was kept flat for comparison (Figure S1-b). The relative roughness height δ^* was defined as:

$$\delta^* = \frac{h}{R_0} \quad (1)$$

Here, R_0 = 75 μm denotes the radius for circular roughness elements and the half height of the equilateral triangle for angular roughness elements (Figure S1-c). h denotes the height of each roughness. For each roughness shape (round and angular), three relative roughness heights δ^* = 0.67 (h_1 = 50 μm), 1.33 (h_2 = 100 μm), and 1.80 (h_3 = 135 μm) were considered (Figure S1-d). The central distance between neighboring roughness elements (round and angular) was kept at d = 100 μm (Figure S1-d).

Confocal Microscopy. The development of biofilms on the boundaries of the microfluidic channel were visualized using a Nikon C2+ confocal laser scanning microscope (CLSM) with 0.31 μm-horizontal resolution and 0.82 μm-vertical resolution. The wavelength of the laser used here is 488 nm. One typical image represents one horizontal scan with 2048 by 2048 pixels, and the biofilms over the channel depth were scanned at 7 vertical positions using the Z-stack function of the Nikon NIS-Elements software. The biofilm cross-sectional images at the middle depth of the channel were used in our analysis. The objective magnification was 10X and 20X. During the experiment, the images were scanned at 30-minute intervals over 24 hours. At each time step, we imaged biofilms at the inlet, outlet, and middle location of the channel.

Image Analysis. Images obtained from CLSM were saved on a HP-Z4-G4 workstation. To calculate the biofilm thickness on the boundaries, we first converted the confocal images to gray scale images and determined the threshold of color difference between biofilm boundary and

water in Image-J (Figure S1-b). Then, we applied this threshold to determine the boundaries of the biofilms after subtracting the biofilm images with the background image (the first image of the time series experiments) using MATLAB. Afterwards, the pixel intensities of the biofilm were summed up and the average biofilm thickness h_B was determined by dividing the total pixel intensities by the length of the field of view.

Numerical Simulation. We simulated the flow in the microfluidic channel in two dimensions using computational fluid dynamics (CFD) finite-element simulation software, COMSOL Multiphysics 5.5 (Burlington, MA, USA). The geometry of the microfluidic channel was set the same as our experimental setup. The Navier-Stokes equation was numerically solved for flow velocity profiles inside the channel using no-slip boundary conditions on all solid surfaces. The stationary simulation was conducted in the fluid phase. Fully developed flow was assumed at the inflow and zero pressure was used at the outflow. Shear stress distribution was calculated based on the velocity profiles. The spatially-averaged shear stress τ_{avg} is defined as the mathematical mean value of the shear stress over the whole channel domain, which was calculated based on the shear stress distribution. The mesh is composed of domain elements ranging in size from 61784 to 90788. The mesh area ranges from 1.63 to 2.03 mm^2. The average quality of an element is around 0.85. More physical parameters used in COMSOL simulation are in the SI (Table S1)

Statistical Analysis. The results of biofilm thickness are shown as mean ± standard error. The mean value of the biofilm thickness was calculated from the inlet, outlet, and middle part of the microfluidic channel. One biological replicate was conducted at the flow rates of 1 μL/min, 5 μL/min, 75 μL/min, and 125 μL/min for all the roughness types. The error bars indicate standard

error of three measurements. Regression analysis was conducted using MATLAB to predict the critical shear stress under different roughness types and find the confidence level. See the SI (Table S2) for more details.

RESULTS AND DISCUSSION

Impacts of Hydrodynamic Conditions on Biofilm Thickness. To reveal the impacts of hydrodynamic conditions on the development of *P. putida* biofilms, we grew *P. putida* cells on the flat surface of custom-built microfluidic channels and measured the thickness of biofilms on the boundary as a function of bacterial growth time (Figure 1). Specifically, we first seed the microfluidic channel with *P. putida* cells by injecting bacterial solution into the microfluidic chamber with flat boundaries. Then, we switched to inject the nutrient solution (M9 medium with 1 wt. % glucose) continuously to allow the cells to grow and biofilms to develop. During the biofilm growth period, we scanned the microfluidic channel using a Confocal Laser Scanning Microscope (CLSM) and measured the average biofilm thickness over time at seven different flow rates (from 1 μL/min to 125 μL/min) (Figure S3). Our results show that biofilms started to form on the boundaries after 6 to 8 hours of nutrient injection. At low flow rate (e.g., 1 ul/min), biofilm clogging was observed after 14 hours (Figure S4). In the following paragraphs, we discuss the impacts of flow on biofilm development before 14-hour growth time.

First, we demonstrate the impacts of flow rate on the thickness of biofilms developed on the flat boundary. At the low flow rate range (1 μL/min to 5 μL/min), we observed rapid increase in biofilm thickness over the 14-hour growth time (Figure 1-a). The biofilm thickness increased exponentially from 8 to 14 hours, indicating that biofilm development is contributed by exponential increase of cell density during the growth phase[11] (Figure S5). At middle flow rate range (15 μL/min to 25 μL/min), the biofilm thickness did not increase exponentially over time and was smaller than the thickness of those grown under the low flow rate range. At the high flow rate range (50 μL/min to 125 μL/min), no biofilm was observed at the boundary, namely biofilm ceased to develop at high flow (>50 μL/min). The prevention of biofilm development by

high flow is likely because bacterial cells can be swept away by flow and detach from surfaces when the flow velocity or shear stress is higher than a critical value.

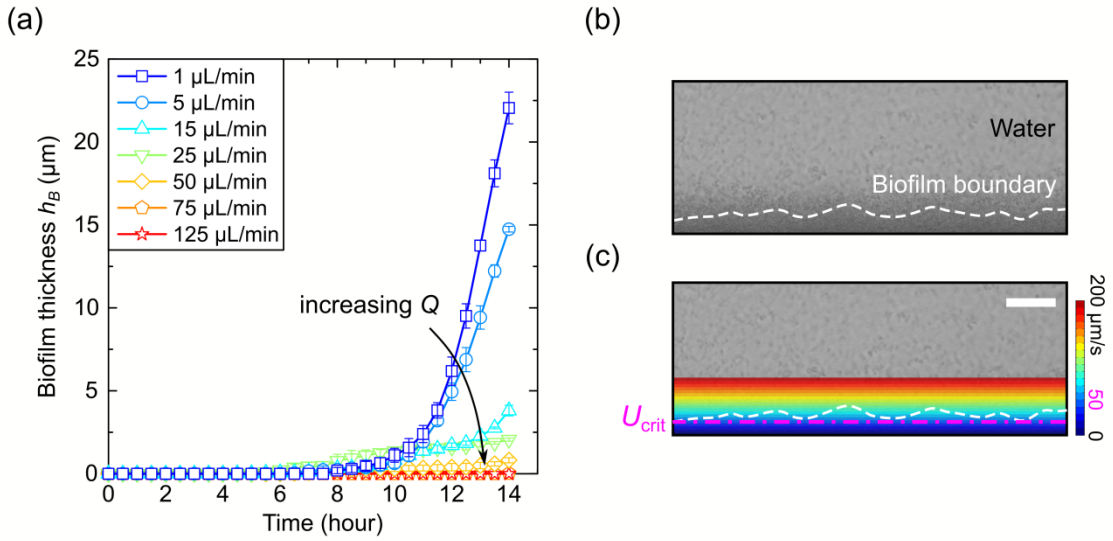

Figure 1. (a) The thickness of *P. putida* biofilms developed on the flat surface of a microfluidic channel (shown in (b)) as a function of time. (b) Confocal microscopic image of biofilms (dark gray color) developed on the flat surface of the microfluidic channel. The white dashed curve denotes the boundary of the biofilm accumulation region identified based on contrast of pixel intensity. The flow rate is Q = 1 μL/min. (c) Flow velocity distribution in color superimposed on gray-scale confocal image shown in (b). The pink dot-dashed line denotes the line with velocity equal to 50 μm/s, which is the local critical velocity for biofilm to develop U_{crit}. The scale bar is 25 μm.

Second, we quantify the local critical conditions for *P. putida* biofilms to develop, by combining the experimental results with numerical simulation of the flow field in the microfluidic channel using COMSOL (Figure 1-b, c). By comparing the CLSM images of biofilms with the flow field simulation, we found that biofilms (with boundary indicated by the

white dashed lines in Figure 1-b, c) accumulated at regions with flow velocity lower than 50 μm/s (the pink lines in Fig. 1-c), suggesting that the local critical velocity for the *P. putida* biofilms to develop is around U_{crit} = 50 μm/s. Furthermore, we conducted the same analysis for channels with varying roughness types at different flow rates (Figure 2-b) and found that U_{crit} = 50 μm/s regardless of flow rates and surface roughness. This indicates that the local critical velocity for *P. putida* biofilms to develop is always 50 μm/s and not affected by boundary roughness. We caution that U_{crit} may be different for different bacterial strains due to the difference in growth rates and bacterial biofilm cohesion abilities.

Impacts of Roughness Heights on Biofilm Thickness. Next, we evaluate the impact of surface roughness on biofilm growth by comparing the development of biofilms on surfaces of varying roughness in microfluidic channels (Figure S3 and S6). Specifically, we measured the time evolution of the average thickness of biofilms developed on flat surfaces and surfaces with round and angular roughness elements of varying heights (Figure 2-a). The average biofilm thickness was defined as the effective thickness assuming a flat surface, i.e., equal to the area of biofilm in 2D divided by the straight-line length of the boundary. As shown in Figure 2-a, biofilms developed on rough surfaces have larger average thickness than those developed on flat surfaces. Furthermore, for the same roughness shape (round or triangular), the average biofilm thickness increases with increasing relative roughness height δ^*. The increase in average biofilm thickness with increasing roughness height is likely caused by the increase in the area of low flow velocity regions induced by the roughness. Above a flat surface, the streamline is parallel to the boundary (Figure 1-c), such that the region with velocity smaller than U_{crit}, the local critical velocity for biofilm to develop, is a thin rectangular region near the flat surface. In comparison,

in channels with rough surfaces, the region with velocity smaller than U_{crit} include the sheltered regions between the roughness elements, which allow more bacterial cells to attach to the surface and form biofilms (Figure 2-b).

In short, we demonstrated that micro-scale surface roughness promotes biofilm formation, i.e., increases average biofilm thickness, by increasing the area of low-velocity region which provides shelter for the bacteria to form biofilms. We caution that the effect of nanoscale roughness may be different because some studies showed higher nanoscale surface roughness reduce bacterial adhesion and inhibit biofilm formation[27, 28].

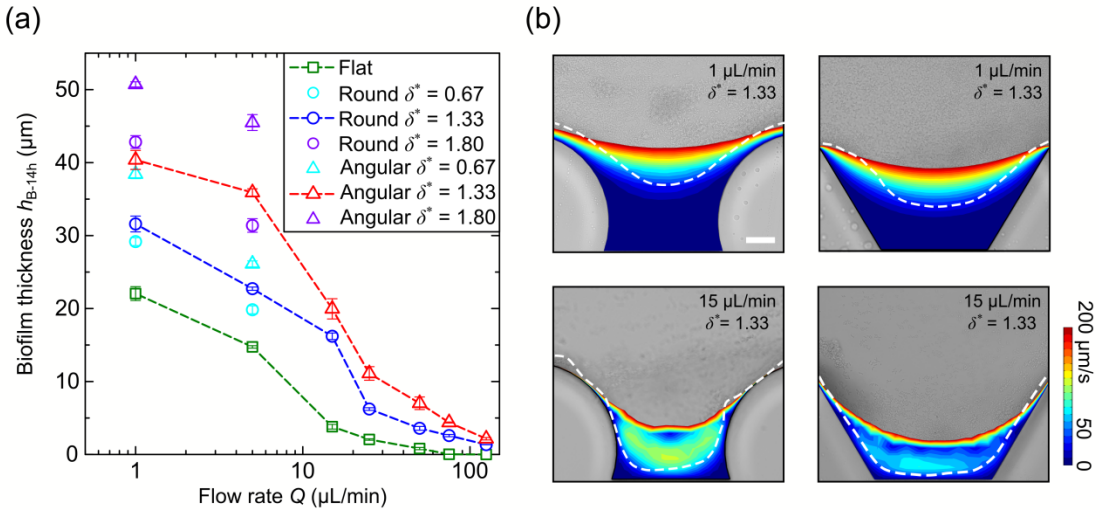

Figure 2. (a) The average thickness of *P. putida* biofilms developed on flat and rough surfaces with round and angular elements at varying flow rates. The symbols and error bars represent the mean value and standard error of the biofilm thickness obtained from four replicate measurements/experiments respectively. (b) Images of flow velocity in color superimposed on gray-scale confocal images of biofilms on surfaces with varying roughness at varying flow velocity: (from left to right) relative roughness height $\delta^* = 1.33$, flow rate $Q = 1$ μL/min, round shape; $\delta^* = 1.33$, $Q = 1$ μL/min, angular shape; $\delta^* = 1.33$, $Q = 15$ μL/min, round shape; $\delta^* =$

1.33, Q = 15 μL/min, angular shape. The white dashed lines denote the boundary of biofilms identified based on contrast of pixel intensity. The scale bar is 25 μm.

Impacts of Roughness Shapes on Biofilm Thickness. Furthermore, we evaluate the impacts of roughness shape on biofilm development. For the same relative roughness height δ^*, the average thickness of biofilms developed on surfaces with angular roughness elements is consistently larger, by up to about 2 times than that for surfaces with round roughness (Figure 2-a), suggesting that surfaces with angular roughness can further promote biofilm formation compared with round shape.

To demonstrate how roughness shape impacts biofilm development, we simulated the shear stress distribution in channels with the round and angular roughness using COMSOL (Figure 3-a, b). In channels with angular roughness element, the higher shear stress region (shear stress > 0.025 Pa, indicated by the red dot-dashed line in Figure 3-a, b) only exists at the peak of the angular roughness element. In contrast, in channels with round roughness, the higher shear stress region extends from the peak location to the middle region of two adjacent cylinders. In the middle region between two adjacent roughness elements (relative location between 0.3 and 0.7), the amount of biofilm accumulation in channel with round roughness is 1.3 times larger than that in the channel with angular roughness (Figure 3-e). However, outside the middle region, or in the "near-peak" regions, the amount of biofilm accumulated in channel with angular roughness is 4.7 times larger than that in channel with round roughness, which is why overall there are 60% more biofilms developed on the surface with angular roughness than on the surface with round roughness. The more abundant biofilms in channels with angular roughness can also be explained by the geometry itself, because the area of the sheltered region between tightly-packed

angular roughness is 2.6 times the area between round roughness (dark blue color in Figure 3-f). Larger sheltered areas have been anticipated to promote biofilm development by increasing the nutrient circulation and mass transport[45]. In short, we found that channels with angular roughness have larger biofilm thickness due to larger areas of low shear stress region between roughness elements, which provide more shelter for bacteria to form biofilm.

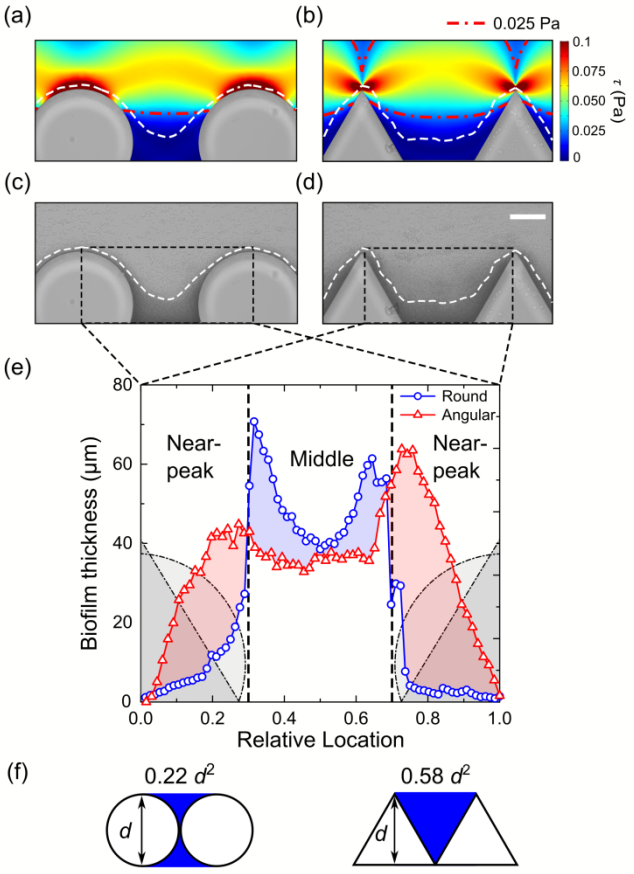

Figure 3. Simulated shear stress distribution (a and b) in color superimposed on gray-scale confocal images (c and d) of biofilms in microfluidic channels with round and angular roughness elements ($\delta^* = 1.33$, $Q = 5$ μL/min). The white dashed curve denotes the boundary of the biofilm. The red dot-dashed line shows the contour of $\tau = 0.025$ Pa based on the simulation. The scale bar is 50 μm. (e) The distribution of the biofilm thickness between the centers of neighboring roughness elements in the dashed boxes region shown in (c) and (d). The light blue area shows

the difference in the amount of biofilm accumulation in the middle part of the channel (relative location between 0.3 and 0.7, the black dashed lines indicate the boundary between "near-peak" region and middle part) between the surface with round and angular roughness. The light red area shows the difference in the amount of biofilm accumulation in the "near-peak" region. The grey areas show the contour of the round and angular roughness shapes. (f) Schematic diagrams of the sheltered region (dark blue color) between tightly-packed round and angular roughness elements.

Impacts of Roughness on Critical Conditions of Biofilm Development. Finally, we reveal the impacts of roughness on the spatially-averaged critical shear stress τ_{crit}, above which biofilms cease to develop.

First, we combine theories and simulation to calculate τ_{crit} for biofilms to develop on a flat surface from U_{crit}, which is the local critical velocity for biofilms to develop and equals to 50 μm/s for *P. putida*. For the experiments in which bacterial solution was injected into the microfluidic channel with width D and flat boundaries at flow rate Q, the Reynolds number ($\mathrm{Re} = \frac{\rho U D_h}{\mu}$, ρ is the density of water, U is the velocity at the inlet, D_h is the hydraulic diameter, μ is the dynamic viscosity of water) is at the range of 0.09 to 11.3, thus the flow is laminar. Assuming a fully developed flow, the velocity profile in the channel can be described by Hagen-Poiseuille flow, i.e., with parabolic distribution[46, 47]:

$$U = \frac{3Q[1-(2y/D)^2]}{2A} \quad (2)$$

where $A = 0.024$ mm^2 is the cross-section area of the channel.

Consider biofilms only develop in regions with velocity less than U_{crit} (Figure 1-c), then the thickness of biofilms, h_B, on the flat boundary can be estimated by substituting U_{crit} into equation (2):

$$h_B = \frac{D}{2} - \frac{D}{2}\sqrt{1 - \frac{2U_{crit}A}{3Q}} \quad (3)$$

We assume that no biofilm will develop on the flat surface when the thickness of this low velocity biofilm zone h_B is less than 1/5 of the bacterial body length, which is 0.1 μm for *P. putida* [48]. Substitute $h_B = h_{crit} = 0.1$ μm into equation (3), we found the critical flow rate Q_{crit} for *P. putida* biofilms to develop is:

$$Q_{crit} = \frac{2U_{crit}A}{3[1-(1-2h_{crit}/D)^2]} \quad (4)$$

Therefore, based on the parabolic velocity distribution (Equation 2), the critical shear stress τ_{crit} to develop biofilms is:

$$\tau_{crit\text{-}theo} = \mu \left.\frac{dU}{dy}\right|_{y=D/2} = \frac{6\mu Q_{crit}}{AD} \quad (5)$$

By using equation (5), we predict that the theoretical critical shear stress for *P. putida* biofilms to develop is $\tau_{crit\text{-}theo} = 0.4$ Pa. To test the validity of our critical shear stress theory (Equations 2-5), we compared the predicted critical shear stress $\tau_{crit\text{-}theo} = 0.4$ Pa with the critical stress estimated from our measurements. Specifically, we plotted the average biofilm thickness at 14-hour growth-time, $h_{B\text{-}14h}$, measured from confocal images, versus the shear stress τ_{avg} calculated from the CFD simulation results (Figure 4-b). Our results show that $h_{B\text{-}14h}$ and τ_{avg} are linearly dependent and above a certain critical shear stress, no biofilms were observed on the surface. To estimate this critical shear stress, we fitted a linear line (blue line in Figure 4-b) to the $h_{B\text{-}14h}$ versus τ_{avg} data and found that the x-intercept, which represents the critical shear stress $\tau_{crit\text{-}exp}$,

and is 0.3 Pa for the flat surface. The agreement between $\tau_{crit\text{-}exp}$ = 0.3 Pa based on measurements and the $\tau_{crit\text{-}theo}$ = 0.4 Pa based on theoretical calculation confirms our hypothesis that the critical conditions to develop biofilms is controlled by local flow velocity. Our predicted and measured τ_{crit} is also consistent with a previous study, which shows that the critical shear stress for microalgae *Chlorella vulgaris* biofilms to develop on the surface of flat-panel photobioreactor is 0.2 Pa[49].

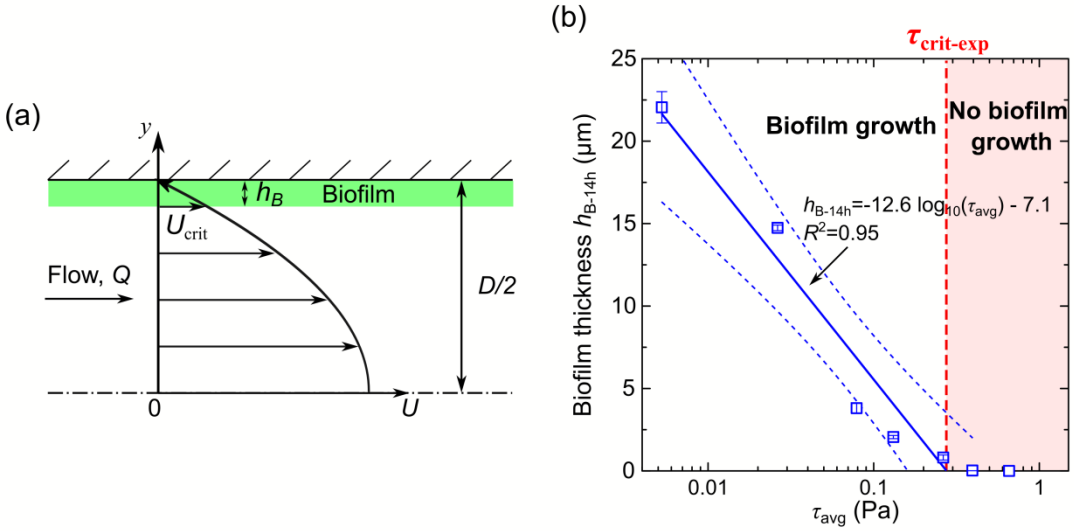

Figure 4. (a) Schematic diagram of the theoretical parabolic velocity distribution (black curve, Equation 2) in the microfluidic channel with flat surfaces. U_{crit} denotes the local critical velocity for biofilms to develop and h_B denotes the biofilm thickness. The light green color represents the region where bacterial biofilms accumulate. (b) The biofilm thickness $h_{B\text{-}14h}$ measured from confocal images (after 14-hour growth period) as a function of the shear stress τ_{avg} calculated from CFD simulation. The red dashed line indicates the critical shear stress τ_{crit}, above which biofilms do not develop on the flat surface. The solid blue line indicates the linear fit $h_{B\text{-}14h}$ = -12.6 log$_{10}$ (τ_{avg}) - 7.1. The blue dashed line represents the 90 % confidence interval.

Furthermore, we demonstrate the impact of surface roughness on τ_{crit}. We plotted the average biofilm thickness as a function of the average shear stress (Figure 5) and identified τ_{crit} for each rough surface. Compared with the flat surfaces for which the measured $\tau_{crit\text{-}flat}$ = 0.3 Pa, the τ_{crit} for biofilms to develop on surfaces with round roughness with δ^* = 1.33 is 0.8 Pa, and on surfaces with angular roughness with δ^* = 1.33 is 0.9 Pa. Therefore, the critical shear stress τ_{crit} for biofilms to develop on surfaces with angular and round roughness is about 3 times as large as that for flat surfaces. Our results highlight the important role of surface roughness on biofilm development.

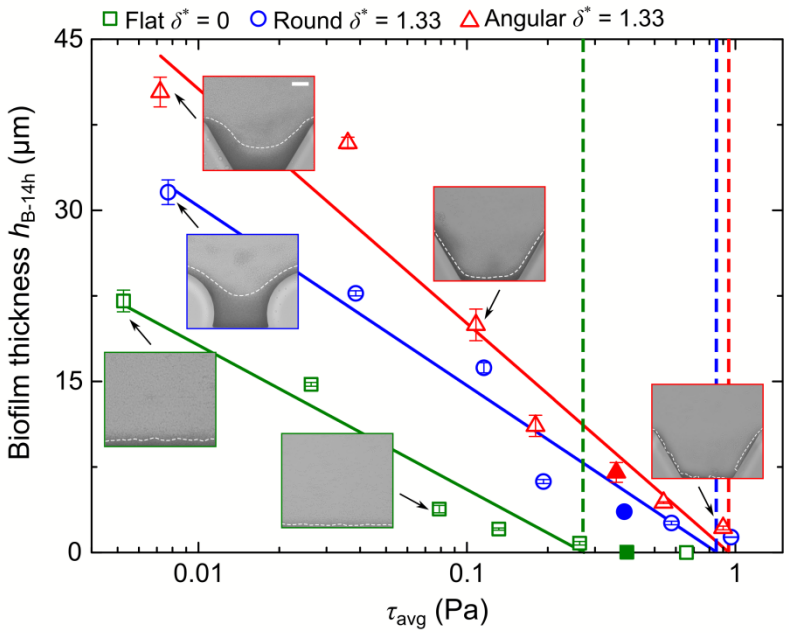

Figure 5. Measured biofilm thickness after 14-hour growth period as a function of shear stress τ_{avg} for flat surface (green) and rough surfaces with round elements (blue) and angular elements (red). The dashed vertical lines indicate the critical shear stress for the flat surface $\tau_{crit\text{-}flat}$ (green), and surfaces with round roughness $\tau_{crit\text{-}round}$ (blue) and angular roughness $\tau_{crit\text{-}angular}$ (red). The three symbols filled with color represent the data (τ_{avg} = 0.38 ± 0.02 Pa) used for Figure 6. The insets

351 show confocal images for representative cases indicated by the black arrows. The scale bar is 25
352 μm for both insets.
353
354 At about the same shear stress conditions, e.g., τ_{avg} = 0.38 ± 0.02 Pa, we anticipate that no
355 biofilm would developed on the flat surface, because the τ_{avg} is larger than $\tau_{crit\text{-}flat}$ = 0.3 Pa (Figure
356 6). In contrast at the same shear stress τ_{avg} = 0.38 ± 0.02 Pa, we predict that biofilms would
357 develop on the rough surfaces with both angular and round roughness elements, because the τ_{avg}
358 is smaller than $\tau_{crit\text{-}rough}$ = 0.8-0.9 Pa. Our predictions are confirmed by our microfluidic
359 observations of biofilms developed on flat and rough surfaces under similar average shear stress
360 (τ_{avg} = 0.38 ± 0.02 Pa), as shown in Fig. 6, suggesting that surface roughness indeed increases τ_{crit},
361 making it more difficult to prevent biofilm growth on rough surfaces by increasing flow velocity.
362 Additionally, our results suggest that a higher shear stress or flow rate is required to prevent
363 biofilm formation on rough surfaces, such as rough surfaces of angular sediment deposits in
364 fluvial system[2], drinking water pipes[7], and MBBRs used in wastewater treatment plants[33].

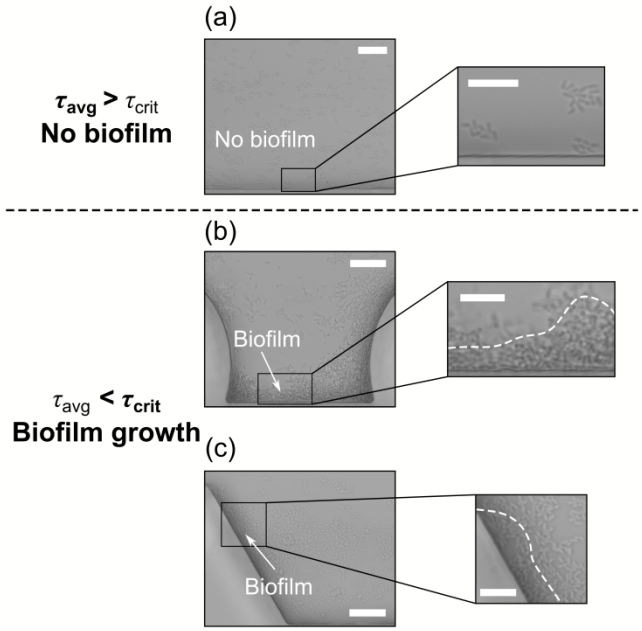

365

Figure 6. The development of biofilms on flat and rough surfaces under similar average shear stress (τ_{avg} = 0.38 ± 0.02 Pa). (a) On the flat surface, no biofilm developed on the boundary because the shear stress in the channel τ_{avg} is larger than the critical shear stress $\tau_{crit\text{-}flat}$ = 0.3 Pa. On surfaces with round roughness (b) and angular roughness (c) with similar shear stress, biofilms can develop on surfaces, as the shear stress τ_{avg} is smaller than the critical shear stress $\tau_{crit\text{-}rough}$ = 0.8-0.9 Pa. The white dashed lines denote the boundary of biofilms. The scale bar is 25 μm. The scale bar of zoom-in images is 10 μm.

In conclusion, we demonstrate the impacts of hydrodynamic conditions and surface roughness on the thickness of and the critical conditions to develop *P. putida* biofilms through systematically-controlled microfluidic experiments and CFD simulations. First, we show that biofilm growth is suppressed under high flow velocity. By combining experimental and simulation results, we demonstrate that the local critical velocity for *P. putida* biofilms to develop is 50 μm/s, and this critical value is the same for the range of flow rates (1 μL/min-125 μL/min) and roughness considered here. Furthermore, we propose a theoretical model to predict the critical shear stress, above which biofilms ceases to develop on flat surfaces, which is $\tau_{crit\text{-}flat}$ = 0.3 Pa. In addition, we revealed the impacts of roughness, including its height and shape, on the biofilm formation. We show that roughness elements create sheltered low flow regions that promote biofilm formation. Compared with round roughness elements, angular roughness elements provide larger area of low flow region, which further facilitate biofilm accumulation. Finally, we demonstrate that the critical shear stress for biofilm to develop on rough surfaces with angular and round roughness is 0.9 Pa and 0.8 Pa, respectively, which are about 3 times higher than that on flat surfaces (0.3 Pa).

389 Our study highlights the important role of hydrodynamic conditions and surface roughness in
390 controlling biofilm formation on surfaces and provides systematic and quantitative
391 characterization of these effects. While our work only considers the initial stages of the biofilm
392 formation process and a single-species biofilm, we expect that the experimental method and
393 predictive equation developed in this study can be extended to study multi-species biofilms in the
394 future. The bacterium used here, *Pseudomonas putida*, is a common soil bacterium and a widely-
395 used strain in bioremediation. Therefore, the results presented here have important implications
396 in predicting and controlling biofilm-related contaminants in aquatic and terrestrial environments
397 as well as in bioremediation industries. Specifically, our results can be used to determine the
398 optimal flow rates to mitigate biofouling in drinking water distribution systems, predict the
399 existence and thickness of biofilms on aquatic sediment and terrestrial soil, as well as facilitate
400 selection of surface roughness and flow velocity to control the thickness of biofilms in MBBRs
401 to optimize bioremediation efficiency.

AUTHOR INFORMATION

Corresponding Author

*Judy Q. Yang (judyyang@umn.edu)

Author Contributions

G.W. and J.Q.Y. conceived and designed the project. G.W. and J.Q.Y. designed the experiments. G.W. conducted the experiments. G.W. and J.Q.Y. analyzed the data and wrote the paper.

Funding Sources

This study was supported by MnDRIVE Environment at the University of Minnesota.

Notes

The authors declare no competing financial interest.

Data Availability Statements

Data will be made available in the Data Repository for University of Minnesota repository (https://doi.org/10.13020/afnk-kp31).

Acknowledgment

We thank Dr. J Sanfilippo for help with the strains. Portions of this work were conducted in the Minnesota Nano Center, which is supported by the National Science Foundation through the National Nanotechnology Coordinated Infrastructure (NNCI) under Award Number ECCS-2025124.

Briefs

Abstract Graphic:

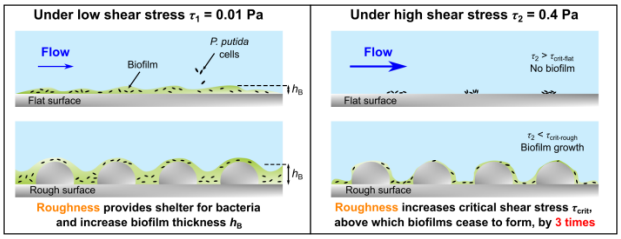

Synopsis

This study demonstrates that microscale surface roughness can increase the critical shear stress to form biofilms by 3 times.

References:

(1) Donlan, R.M. Biofilms: microbial life on surfaces. *Emerg. Infect. Dis.* 2002, *8*(9), 881.

(2) Risse-Buhl, U.; Anlanger, C.; Kalla, K.; Neu, T.R.; Noss, C.; Lorke, A.; Weitere, M. The role of hydrodynamics in shaping the composition and architecture of epilithic biofilms in fluvial ecosystems. *Water Res.* 2017, *127*, 211-222.

(3) Drummond, J.D.; Davies-Colley, R.J.; Stott, R.; Sukias, J.P.; Nagels, J.W.; Sharp, A.; Packman, A.I. Microbial Transport, Retention, and Inactivation in Streams: A Combined Experimental and Stochastic Modeling Approach. *Environ. Sci. Technol.* 2015, *49*(13), 7825-7833.

(4) Tlili, A.; Corcoll, N.; Arrhenius, Å.; Backhaus, T.; Hollender, J.; Creusot, N.; Wagner, B.; Behra, R. Tolerance patterns in stream biofilms link complex chemical pollution to ecological impacts. *Environ. Sci. Technol.* 2020, *54*(17), 10745-10753.

(5) De Carvalho, C.C. Marine biofilms: a successful microbial strategy with economic implications. *Frontiers in marine science*. 2018, *5*, 126.

(6) Schulze, A.; Mitterer, F.; Pombo, J.P.; Schild, S. Biofilms by bacterial human pathogens: Clinical relevance-development, composition and regulation-therapeutical strategies. *Microbial Cell*. 2021, *8*(2), 28.

(7) Fish, K.; Osborn, A.M.; Boxall, J.B. Biofilm structures (EPS and bacterial communities) in drinking water distribution systems are conditioned by hydraulics and influence discolouration. *Sci. Total Environ.* 2017, *593-594*, 571-580.

(8) Shen, Y.; Huang, C.; Monroy, G.L.; Janjaroen, D.; Derlon, N.; Lin, J.; Espinosa-Marzal, R.; Morgenroth, E.; Boppart, S.A.; Ashbolt, N.J. Response of simulated drinking water biofilm mechanical and structural properties to long-term disinfectant exposure. *Environ. Sci. Technol.* 2016, *50*(4), 1779-1787.

(9) September, S.M.; Els, F.A.; Venter, S.N.; Brözel, V.S. Prevalence of bacterial pathogens in biofilms of drinking water distribution systems. *J. Water Health*. 2007, *5*(2), 219-227.

(10) Donlan, R.M. Biofilms and device-associated infections. *Emerg. Infect. Dis.* 2001, *7*(2), 277.

(11) Drescher, K.; Shen, Y.; Bassler, B.L.; Stone, H.A. Biofilm streamers cause catastrophic disruption of flow with consequences for environmental and medical systems. *Proceedings of the National Academy of Sciences*. 2013, *110*(11), 4345-4350.

(12) Dressaire, E.; Sauret, A. Clogging of microfluidic systems. *Soft Matter*. 2017, *13*(1), 37-48.

(13) Ghannoum, M.; Parsek, M.; Whiteley, M.; Mukherjee, P.K. *Microbial biofilms*, John Wiley & Sons, 2020.

(14) Bassin, J.P.; Kleerebezem, R.; Rosado, A.S.; van Loosdrecht, M.M.; Dezotti, M. Effect of different operational conditions on biofilm development, nitrification, and nitrifying microbial population in moving-bed biofilm reactors. *Environ. Sci. Technol.* 2012, *46*(3), 1546-1555.

(15) Zhu, I.X.; Getting, T.; Bruce, D. Review of biologically active filters in drinking water applications. *Journal - American Water Works Association*. 2010, *102*(12), 67-77.

(16) Torresi, E.; Fowler, S.J.; Polesel, F.; Bester, K.; Andersen, H.R.; Smets, B.F.; Plosz, B.G.; Christensson, M. Biofilm Thickness Influences Biodiversity in Nitrifying MBBRs Implications on Micropollutant Removal. *Environ. Sci. Technol.* 2016, *50*(17), 9279-9288.

(17) Suarez, C.; Piculell, M.; Modin, O.; Langenheder, S.; Persson, F.; Hermansson, M. Thickness determines microbial community structure and function in nitrifying biofilms via deterministic assembly. *Sci. Rep.-UK*. 2019, *9*(1), 1-10.

(18) Krsmanovic, M.; Biswas, D.; Ali, H.; Kumar, A.; Ghosh, R.; Dickerson, A.K. Hydrodynamics and surface properties influence biofilm proliferation. *Adv. Colloid Interfac.* 2021, *288*, 102336.

(19) Zheng, S.; Bawazir, M.; Dhall, A.; Kim, H.; He, L.; Heo, J.; Hwang, G. Implication of surface properties, bacterial motility, and hydrodynamic conditions on bacterial surface sensing and their initial adhesion. *Frontiers in Bioengineering and Biotechnology*. 2021, *9*, 82.

(20) Cowle, M.W.; Webster, G.; Babatunde, A.O.; Bockelmann-Evans, B.N.; Weightman, A.J. Impact of flow hydrodynamics and pipe material properties on biofilm development within drinking water systems. *Environ. Technol.* 2019.

(21) Liu, N.; Skauge, T.; Landa-Marbán, D.; Hovland, B.; Thorbjørnsen, B.; Radu, F.A.; Vik, B.F.; Baumann, T.; Bødtker, G. Microfluidic study of effects of flow velocity and nutrient concentration on biofilm accumulation and adhesive strength in the flowing and no-flowing microchannels. *Journal of Industrial Microbiology and Biotechnology*. 2019, *46*(6), 855-868.

(22) Paramonova, E.; Kalmykowa, O.J.; Van der Mei, H.C.; Busscher, H.J.; Sharma, P.K. Impact of hydrodynamics on oral biofilm strength. *J. Dent. Res.* 2009, *88*(10), 922-926.

(23) Lemos, M.; Mergulhão, F.; Melo, L.; Simões, M. The effect of shear stress on the formation and removal of *Bacillus cereus* biofilms. *Food Bioprod. Process.* 2015, *93*, 242-248.

(24) Shen, Y.; Monroy, G.L.; Derlon, N.; Janjaroen, D.; Huang, C.; Morgenroth, E.; Boppart, S.A.; Ashbolt, N.J.; Liu, W.T.; Nguyen, T.H. Role of biofilm roughness and hydrodynamic conditions in *Legionella pneumophila* adhesion to and detachment from simulated drinking water biofilms. *Environ. Sci. Technol.* 2015, *49*(7), 4274-4282.

(25) Yoda, I.; Koseki, H.; Tomita, M.; Shida, T.; Horiuchi, H.; Sakoda, H.; Osaki, M. Effect of surface roughness of biomaterials on *Staphylococcus epidermidis* adhesion. *BMC Microbiol.* 2014, *14*(1), 1-7.

(26) Bollen, C.M.; Papaioanno, W.; Van Eldere, J.; Schepers, E.; Quirynen, M.; Van Steenberghe, D. The influence of abutment surface roughness on plaque accumulation and peri‐implant mucositis. *Clin. Oral Implan. Res.* 1996, *7*(3), 201-211.

(27) Wu, S.; Altenried, S.; Zogg, A.; Zuber, F.; Maniura-Weber, K.; Ren, Q. Role of the surface nanoscale roughness of stainless steel on bacterial adhesion and microcolony formation. *ACS omega.* 2018, *3*(6), 6456-6464.

(28) Matalon, S.; Safadi, D.; Meirowitz, A.; Ormianer, Z. The effect of aging on the roughness and bacterial adhesion of lithium Disilicate and Zirconia ceramics. *Journal of Prosthodontics.* 2021, *30*(5), 440-446.

(29) Hryciw, R.D.; Zheng, J.; Shetler, K. Particle roundness and sphericity from images of assemblies by chart estimates and computer methods. *J. Geotech. Geoenviron.* 2016, *142*(9), 4016038.

(30) Miller, K.L.; Szabó, T.; Jerolmack, D.J.; Domokos, G. Quantifying the significance of abrasion and selective transport for downstream fluvial grain size evolution. *Journal of Geophysical Research: Earth Surface.* 2014, *119*(11), 2412-2429.

(31) Niquette, P.; Servais, P.; Savoir, R. Impacts of pipe materials on densities of fixed bacterial biomass in a drinking water distribution system. *Water Res.* 2000, *34*(6), 1952-1956.

(32) Mahto, K.U.; Das, S. Bacterial biofilm and extracellular polymeric substances in the moving bed biofilm reactor for wastewater treatment: A review. *Bioresource Technol*. 2022, *345*, 126476.

(33) Morgan-Sagastume, F. Biofilm development, activity and the modification of carrier material surface properties in moving-bed biofilm reactors (MBBRs) for wastewater treatment. *Crit*. *Rev*. *Env*. *Sci*. *Tec*. 2018, *48*(5), 439-470.

(34) Brettar, I.; Ramos-Gonzalez, M.I.; Ramos, J.L.; Höfle, M.G. Fate of *Pseudomonas putida* after release into lake water mesocosms: different survival mechanisms in response to environmental conditions. *Microb*. *Ecol*. 1994, *27*(2), 99-122.

(35) Molina, L.; Ramos, C.; Duque, E.; Ronchel, M.C.; García, J.M.; Wyke, L.; Ramos, J.L. Survival of *Pseudomonas putida* KT2440 in soil and in the rhizosphere of plants under greenhouse and environmental conditions. *Soil Biology and Biochemistry*. 2000, *32*(3), 315-321.

(36) Maes, S.; De Reu, K.; Van Weyenberg, S.; Lories, B.; Heyndrickx, M.; Steenackers, H. *Pseudomonas putida* as a potential biocontrol agent against *Salmonella* Java biofilm formation in the drinking water system of broiler houses. *BMC Microbiol*. 2020, *20*(1), 1-13.

(37) Samanta, S.K.; Singh, O.V.; Jain, R.K. Polycyclic aromatic hydrocarbons: environmental pollution and bioremediation. *Trends Biotechnol*. 2002, *20*(6), 243-248.

(38) Ravi, K.; García-Hidalgo, J.; Gorwa-Grauslund, M.F.; Lidén, G. Conversion of lignin model compounds by *Pseudomonas putida* KT2440 and isolates from compost. *Appl*. *Microbiol*. *Biot*. 2017, *101*(12), 5059-5070.

(39) Xu, R.; Zhang, K.; Liu, P.; Han, H.; Zhao, S.; Kakade, A.; Khan, A.; Du, D.; Li, X. Lignin depolymerization and utilization by bacteria. *Bioresource Technol*. 2018, *269*, 557-566.

(40) De, J.; Leonhäuser, J.; Vardanyan, L. Removal of mercury in fixed-bed continuous upflow reactors by mercury-resistant bacteria and effect of sodium chloride on their performance. *QScience Connect*. 2014, *2014*(1), 17.

(41) Imron, M.F.; Kurniawan, S.B.; Soegianto, A. Characterization of mercury-reducing potential bacteria isolated from Keputih non-active sanitary landfill leachate, Surabaya, Indonesia under different saline conditions. *J. Environ. Manage.* 2019, *241*, 113-122.

(42) El-Naas, M.H.; Al-Muhtaseb, S.A.; Makhlouf, S. Biodegradation of phenol by *Pseudomonas putida* immobilized in polyvinyl alcohol (PVA) gel. *J. Hazard. Mater.* 2009, *164*(2-3), 720-725.

(43) Kadivar, M.; Tormey, D.; McGranaghan, G. A review on turbulent flow over rough surfaces: Fundamentals and theories. *International Journal of Thermofluids*. 2021, *10*, 100077.

(44) Sultan, T.; Cho, J. Methodology considering surface roughness in UV water disinfection reactors. *Chem. Pap.* 2016, *70*(6), 777-792.

(45) Percival, S.L.; Knapp, J.S.; Wales, D.S.; Edyvean, R. The effect of turbulent flow and surface roughness on biofilm formation in drinking water. *Journal of industrial Microbiology and Biotechnology*. 1999, *22*(3), 152-159.

(46) Bejan, A. *Convection heat transfer*, John wiley & sons, 2013.

(47) Sutera, S.P.; Skalak, R. The history of Poiseuille's law. *Annu. Rev. Fluid Mech.* 1993, *25*(1), 1-20.

(48) Prieto, A.; Escapa, I.F.; Martínez, V.; Dinjaski, N.; Herencias, C.; de la Peña, F.; Tarazona, N.; Revelles, O. A holistic view of polyhydroxyalkanoate metabolism in *Pseudomonas putida*. *Environ. Microbiol.* 2016, *18*(2), 341-357.

(49) Belohlav, V.; Zakova, T.; Jirout, T.; Kratky, L. Effect of hydrodynamics on the formation and removal of microalgal biofilm in photobioreactors. *Biosyst. Eng.* 2020, *200*, 315-327.